Publishing Excellence Inspiring Progress
ARISTON PUBLICATIONS
MatSci Express
ISSN: 2997-8440 www.aristonpubs.com/matsci-express https://doi.org/10.69626/mse.2025.0113

RESEARCH ARTICLE

Comparative Analysis of Green and Chemical Synthesis Approaches for Lead Ion Detection Using Iron Oxide Nanoparticles

Teenu Jasrotia [2, ‡], Neha Garg [1, ‡], Ganga Ram Chaudhary [1], Savita Chaudhary [1, *], Rajeev Kumar [2,*], Abhijit Dan [3]

ABSTRACT: Lead (Pb^{2+}) contamination poses a significant threat to human health and the environment due to its high toxicity, bioaccumulation, and persistence. The development of efficient and selective sensing mechanisms for Pb^{2+} detection is, therefore, crucial for environmental monitoring and industrial applications. In this study, iron oxide nanoparticles (FeO NPs) were synthesized using both green and chemical methods and employed as fluorescence-based sensors for the selective detection of Pb^{2+} ions in an aqueous medium. The green synthesis method utilized plant-derived extracts, resulting in FePE-NPs, while the chemically synthesized nanoparticles were designated as FeCH-NPs. Comparative analysis demonstrated that FePE-NPs exhibited superior performance, with a lower limit of detection (LOD) of 19.57 nM, compared to 29.43 nM for FeCH-NPs. The FePE-NPs also exhibited greater selectivity for Pb^{2+} over competing metal ions due to their enhanced surface functionality and biocompatibility. Characterization techniques, including UV-vis, FTIR, XRD, DLS, and FE-SEM, confirmed the successful synthesis and stability of the nanoparticles. Additionally, real water sample testing revealed high recovery rates (94–98% for FePE-NPs and 90–97% for FeCH-NPs), further validating their potential for practical applications. The study highlights the advantages of green synthesis, which not only enhances the sensing efficiency but also promotes sustainable and eco-friendly nanoparticle fabrication. The findings suggest that FePE-NPs serve as an efficient, cost-effective, and environmentally friendly sensor for detecting trace levels of lead ions in contaminated water sources, paving the way for future advancements in green nanotechnology for environmental remediation.

Keywords: Iron Oxide Nanoparticles, Lead Ion Detection, Green Synthesis, Fluorescence Sensor, Environmental Monitoring, Heavy Metal Sensing.

Received: 23 August 2024; Revised: 13 October 2024; Accepted: 30 November 2024; Published Online: 13 January 2025

1. INTRODUCTION

Heavy metal ions such as mercury, arsenic, lead, cadmium and chromium have become major environmental contaminants found in air, soil and water sources due to its worst impact on the ecosystem and human health [1-4]. They generally have high water solubility [5], low degradability and high toxicity [6-7]. If these toxic metals exceed a particular level, they have adverse impact on human health [8-11]. Out of them, lead ions (Pd^{2+} ions) are found to be one of the most toxic environmental pollutants even at low concentrations [12-14]. It may cause muscle paralysis, memory loss, anaemia, nervous system dysfunction,

[1] Department of Chemistry, Panjab University, Chandigarh 160014, India
[2] Department of Environmental Studies, Panjab University, Chandigarh 160014, India
[3] Department of Applied Chemistry, Maulana Abul Kalam Azad University of Technology, Simhat, Haringhata, West Bengal 741249, India

* Author to whom correspondence should be addressed: schaudhary@pu.ac.in (S.Chaudhary)
rajeev@pu.ac.in (R. Kumar)

‡ Authors contributed equally to this work.

© Ariston Publications 2025. All rights reserved.

developmental disorders etc [15-18]. Therefore, there is a need to develop selective and sensitive detection method to address the concern of lead toxicity. Till now, many conventional analytical techniques including inductively coupled plasma mass spectrometry (ICP-MS) [19-21], inductively coupled plasma atomic emission spectroscopy (ICP-AES) [22-24], colorimetric method [25-28] and atomic absorption spectroscopy (AAS) [29-32] have been widely adopted for the quantitative and qualitative analysis of lead ions. Also, electrochemical based sensors have been developed for metal ions sensing [33-35]. But they required skilled analysis, sophisticated operators, tedious time, sample pre-treatments and are not so much cost effective. Therefore, the alternative for this tedious job is to employ fluorescence-based sensors due to its low-cost, high efficiency, less time consuming, quick response and ease of functioning [36,37].

Till now, various sensors have been developed for the selective detection of Pb^{2+} ions based upon fluorescence technique. For instance, Saha et al. proposed a conjugated fluorene-based polymer for the selective fluorescence quenching response towards Pb^{2+} over other metal cations in aqueous solution with limit of detection (LOD) value of 4 µM [38]. Zhang et al. designed novel graphitic carbon nitride nanocones based probe for the detection of Pb^{2+} in aqueous media with LOD value of 0.0438 µM [39]. The functionalized molybdenum disulfide (MoS_2) quantum dots (QDs) were developed by Sharma et al. and they are highly selective to Pb^{2+} over other metal ions with LOD value of 50 µM [40]. Tian et al. report a highly fluorescent probe via the immobilization of surface functionalized carbon dots (named as CAEA-Hs) into the shell of the spherical polyelectrolyte brushes for selective recognition of Pb^{2+} in aqueous medium. It shows the LOD value of 22.5 µM [41]. Song et al. developed a fluorescent probe by covalently combining a fluorescent 1,8-naphthalimide dye with cellulose nanocrystals (CNCs) for selective fluorescent detection of Pb^{2+} (detection concentration of 0.15 µM) in water [42]. Shi et al. synthesized nitrogen and sulphur doped carbon quantum dots (N-SCQDs) for sensitive detection of Pb^{2+} ions [43]. The limit of detection was calculated to be 0.097 μM and 5.624 μM in the scope of 0.2-12 μM and 40-200 μM concentration range of Pb^{2+} ions. However, inspite of the significant progress in this field, some challenges are still there that includes high cost of reactant molecules, low sensitivity and chemical instability. In view of this context, the exploration of nanoparticles (Nps) based fluorometric sensors for the highly selective and sensitive determination of Pb^{2+} ions become a topic of significant interest.

While significant advancements have been achieved in detecting heavy metals, the need for a more efficient and cost-effective solution still persists. Now, Nps could be designed by two ways either by green method or by using simple chemical reduction method. It seems to be that the Nps synthesized by green methods shows more efficiency but Nps designed by chemical method are more reliable and accurate. Therefore, in this work we have formulated iron oxide nanoparticles (FeO Nps) using seed extract (green method) as well as chemical reduction method so that it is easy to compare the efficiency of both the Nps for the sensitivity and selectivity sensing towards Pb^{2+} ions.

2. EXPERIMENTAL DETAILS

2.1. Materials

Seeds of *Koelreuteria apiculate* were procured from the botanical garden of the Panjab University. Ferric chloride hexahydrate ($FeCl_3.6H_2O$) salt (97%), Cetyltrimethyl ammonium bromide (CTAB) (*>98%)* and Sodium borohydride ($NaBH_4$) (*>98%)* was obtained from Sigma Aldrich.

2.2. Synthesis of Iron oxide Nanoparticles

The synthesis of iron oxide Nps *via* green method as well as chemical method were carried out using our previously reported method [44, 45]. In brief, the seeds of *Koelreuteria apiculate* were thoroughly washed with deionized water to remove the dust particles present on the surface of seeds. After drying and grinding, seed powder was obtained. Then 5 g of this seed powder was dissolved in 100 mL of deionized water and incubated at 250°C on a heating plate with continuous stirring. Afterwards, it was cool down and filtered through Whatman filter paper. The collected supernatant was centrifuged at 5000 rpm for 5 min. to get pale-yellow colored seed extract. To obtain iron oxide Nps, 10 mM ferric chloride salt were dissolved in 10 mL of deionized water in a separate beaker. To the salt solution, seed extract was added and left undisturbed for 24 h. The precipitation starts as a result of the interactions carried out between the seed extract and metal salt solution. The obtained precipitates were centrifuged at 7000 rpm several times (Figure 1). Then, the precipitates were dried in an oven to obtain iron oxide nanoparticles (FePE-Nps) [44]. Chemically, the synthesis of iron oxide Nps was carried out by a simple chemical precipitation method. For the synthesis purpose, the aqueous solution of 0.05 M of $FeCl_3.6H_2O$ was prepared in 100 mL of deionized water by using 0.03 M CTAB as a surfactant. The obtained solution was stirred for 20 min. with the help of a magnetic stirrer. To the above solution, 10 mL of 0.2% $NaBH_4$ was added dropwise till it changed to the dark-coloured suspension of FeCH-Nps [45]. The Nps precipitated in this process were extracted by centrifugation and provided with multiple washings of deionized water. The collected FeCH-Nps were dried in an oven at 70°C to obtain powdered form (Figure 1).

2.3. Instrumentation

The Ultraviolet-visible (UV-vis.) analysis was performed on LABINDIA UV-visible spectrophotometer. Functional groups determination was carried out using Fourier Transform Infrared Spectroscopy (FTIR) on Perkin Elmer

 © Ariston Publications 2025. All rights reserved.

(RX1) Fourier transform infrared spectrometer. Powder X-ray Diffraction (XRD) analysis was done on Panalytical D/Max 2500 X-ray Diffractometer. The size distribution was performed using Malvern zeta sizer (ZEN 1690). Field Emission-Scanning Electron Microscopy (FE-SEM) was performed on Hitachi Field Emission-Scanning Electron Microscope (FE-SEM) SU8000 spectrometer. High-resolution transmission electron microscopy (HR-TEM) was performed on Hitachi Transmission Electron microscope (TEM) bearing model no. H-7500. REMI R-24 centrifuge was used for centrifugation of samples.

3. RESULTS AND DISCUSSION

3.1. Characterization

The detailed characterizations of the prepared Nps have been carried out previously in our reported work [44, 45]. To elaborate, the UV-vis. spectra shows a peak at the wavelength of 427 nm corresponded to the successful formation of the FePE-Nps. The secondary plant metabolites of the coating material exhibited changes in free electron density as portrayed by the phenomenon of red shift which resulted in the stabilization of FePE-Nps. The appearance of another peak at 535 nm pointed towards the presence of FeO/Wüstite. UV-vis. spectrum of FeCH-Nps showed the absorption peak positioned at 312 nm, thus supporting the formation and stability of the concerned Nps in the aqueous colloidal solution. The SPR property of FeCH-Nps explained the obtained hump. DLS spectrum of the synthesized FeCH-Nps showed a hydrodynamic diameter in the range of 25 nm as evident from the data. The XRD spectra of the FePE-Nps showed the peaks at 17.9°, 25.48°, 31.8°, 35.91°, 41.7° and 54.84° concerned with the respective values of (111), (210), (220), (200), (440) and (422) as Bragg reflection planes. The broadness obtained in the peaks reflected the nanometric range of the synthesized FePE-Nps. These Nps reflected the maghemite symmetry accorded to the JCPDS no. 39-1346 with the crystallite size of around 7 nm as per Debye Scherrer's formula. *For* FeCH-Nps, XRD screening showed the presence of peaks at 30.3°, 35.7°, 43.4°, 53.8°, 57.4°, and 63° corresponded to the respective reflection planes of (220), (311), (400), (422), (511), and (440) coinciding with the JCPDS No. 019-0629. The diffraction patterns exhibited by FeCH-Nps supported the inverse spinel crystalline structure of Fe_3O_4 and maghemite (γ-Fe_2O_3) analogous to the cubic single phase with an average size of 24 nm.

The FTIR spectrum showed the appearance of peaks at 3266, 2923, and 1631 cm^{-1} which were allied to the presence of respective functional groups like stretching of alcoholic and phenolic hydroxyl groups, stretching of carboxylic O-H groups, and weak stretching of alkenes (C=C). The stances of aromatic stretching of C-C and C-N groups were found with the evidence of peaks at 1535 and 1390 cm^{-1} respectively. Apart from these, the peak at 1047 cm^{-1} reflected the ester group (C-O) along with the weak aliphatic amines (C-N) and the peak at 1004 cm^{-1} signified the presence of a stretch of esters (C-O) on the surface of FePE-Nps. These results showed the interactive actions of functional groups present in the *K. apiculata* extract for the synthesis of FePE-Nps. The absorption peaks obtained at 3374, 1622, 989, and 794 cm^{-1} reflected the O-H stretching of alcohol, carboxylic acid together with N-H stretching of amines, C=C stretch of crystalline FeCH-Nps, and aromatic out-of-plane ring bends respectively, thus confirming the structures of aromatic compounds in the FeCH-Nps.

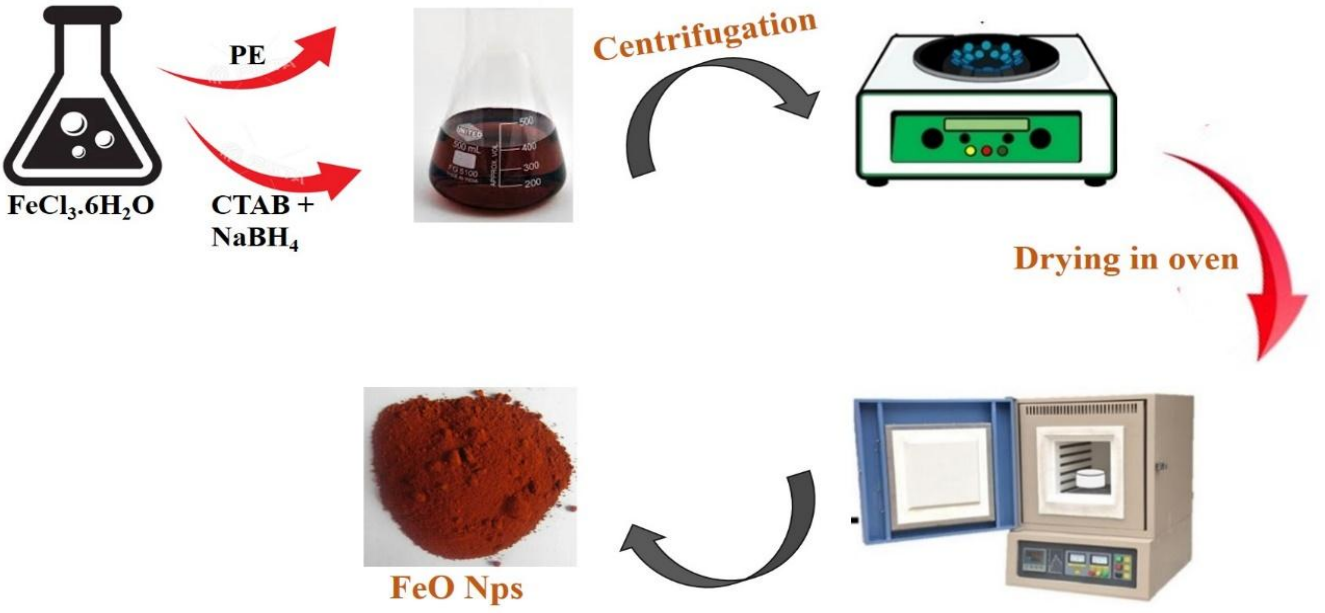


Fig. 1. Schematic illustration of the synthesis process of FePE-Nps and FeCH-Nps.

© Ariston Publications 2025. All rights reserved.

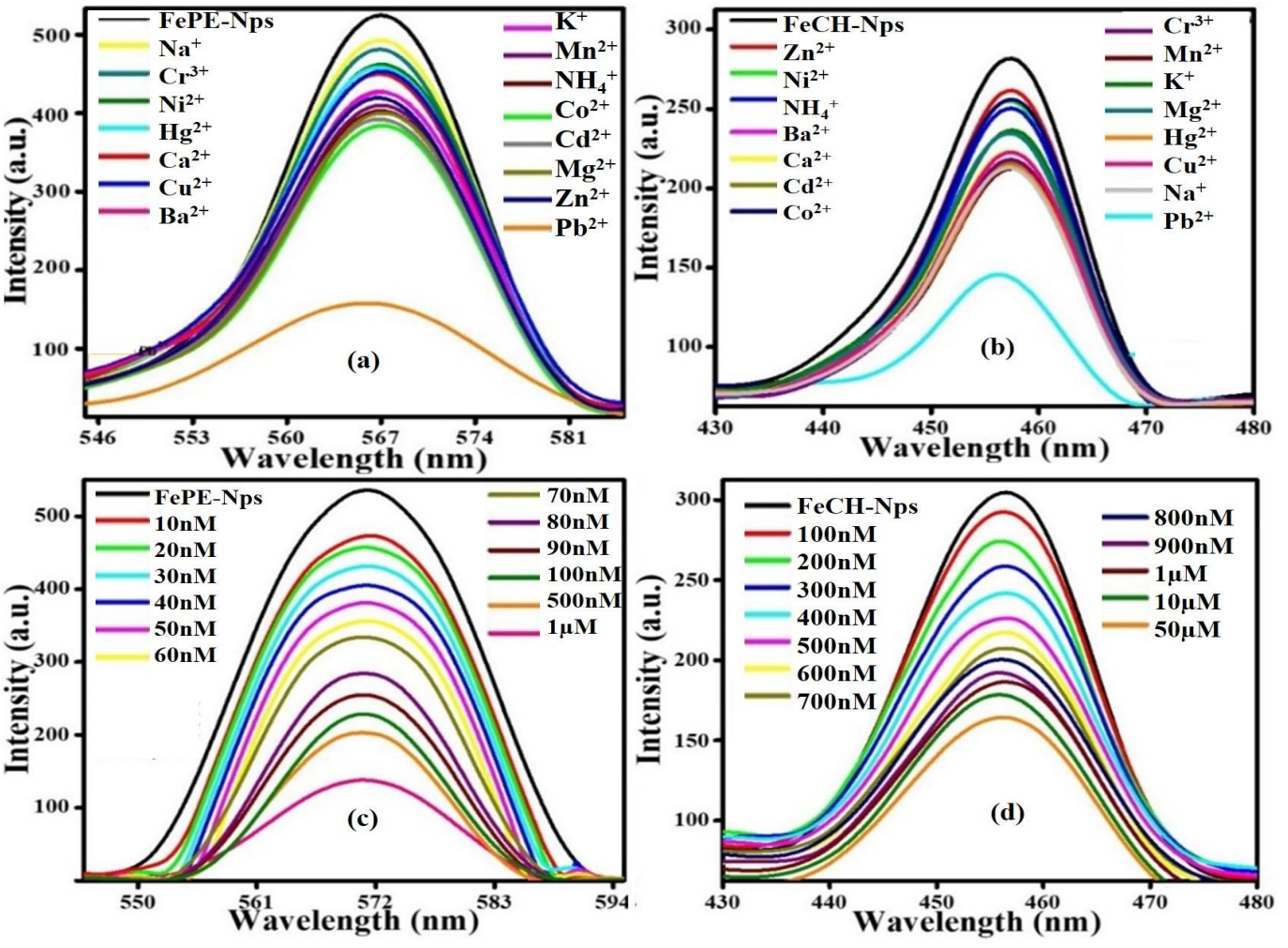


Fig. 2. (a, b) Fluorescence spectra in presence of different metal ions and (c, d) Effect of Pb^{2+} concentration variation for FePE-Nps and FeCH-Nps respectively.

The captured FE-SEM image of the FePE-Nps showed their spherical morphology, formation within the nano-ranges, and fused structures thus explaining the coating of plant extract. The aggregation is evident from the images of FePE-Nps was either attributed to their magnetic nature or their tendency to belittle surface energy associated with them. FePE-Nps were mostly found within the diameter range of 15 nm. FeCH-Nps had spherical morphology with a slight agglomeration tendency. The picture of FE-SEM shows formation of networked spherical structures of FeCH-Nps. The captured HR-TEM image of FeCH-Nps showed an average diameter of 23 nm [44, 45].

3.2. Sensing aptitude towards different metal ions

The increased concentration of metals above the natural level because of the intentional as well as non-intentional extraction processes had disturbed their biogeochemical cycling, thus disturbing nature. There are several metals such as lead, arsenic, and mercury which are having toxicity issues associated with them. Therefore, sensing of these toxic metals is the utmost requirement of the present times.

3.2.1. Fluorescence studies

The fluorescence sensing aptitude of both Nps was checked with different metal ions including Ba^{2+}, K^{+}, NH_4^{+}, Pb^{2+}, Na^{+}, Ni^{2+}, Zn^{2+}, Ca^{2+}, Mg^{2+}, Cu^{2+}, Cr^{2+}, Co^{2+}, Mn^{2+}, Cd^{2+} and Hg^{2+}. The quenching or decrease in the intensity obtained in both spectra showed the potential of Nps for interacting with different metal species. All the metal ions except Pb^{2+} showed only minor changes in the emission intensity, whereas Pb^{2+} acted as the strongest quencher. Both the Nps showed most prominent results with the Pb^{2+} metal ions (Figure 2 (a), (b)). So, utmost attention was paid to investigate the sensitivity of the devised sensors for the

 © Ariston Publications 2025. All rights reserved.

detection of Pb^{2+} ions.

A modified titration-metric approach was employed for the investigation and quantification of the sensitivity of chemosensors. Depending upon the extent of quenching or decrement in the emission intensity of the Nps, various sets of analyte concentrations were selected for different systems. FePE-Nps fluorescence activity was checked against the range of 10 nM-1 µM Pb^{2+} ions concentration (Figure 2(c)) whereas FeCH-Nps activity was monitored for the range varied from 100 nM-50 µM of Pb^{2+} dissolved in solution (Figure 2(d)). In both cases, a linear decrease was observed in the emission intensity of the Nps after mixing with the increased concentrations of metal ions. Thus, reflecting good selectivity and sensitivity towards the selected metal ion. The outcomes also revealed better quenching and hence performance of plant-coated FePE-Nps with lower detection limits than their chemically synthesized counterpart.

The quantitative estimations were made regarding various calculated parameters by using the calibration curves. The Stern-Volmer relationship as explained below in the equation was utilized to quantify the fluorescence quenching in the presence of Pb^{2+} ions.

$$\frac{F_0}{F} = 1 + K_{SV}[Q] \quad (1)$$

Wherein, F_0, F, K_{SV} and Q represent the intensity of Nps, intensity of Nps in presence of Pb^{2+} ions, Stern-Volmer association constant and concentration of Pb^{2+} ions respectively. Figure 3 (a) and (b) show the Stern-Volmer plot for FePE-Nps and FeCH-Nps respectively. The Limit of Detection (LOD) and Limit of Quantitation (LOQ) value was calculated by using a standard formula involving values of the slope of the Stern-Volmer plot (P) and standard deviation (SD) designated as:

$$LOD = \frac{3SD}{P} \quad (2)$$

$$LOD = \frac{10SD}{P} \quad (3)$$

The calculated parameters of LOD and LOQ for FePE-Nps with the value of 19.57 nM and 65.29 nM respectively showed better results than FeCH-Nps with the respective values of 29.43 nM and 98.12 nM for the same set of parameters. Hence, FePE-Nps exhibited more enhanced sensitivity towards the detection of Pb^{2+} ions from the aqueous environment.

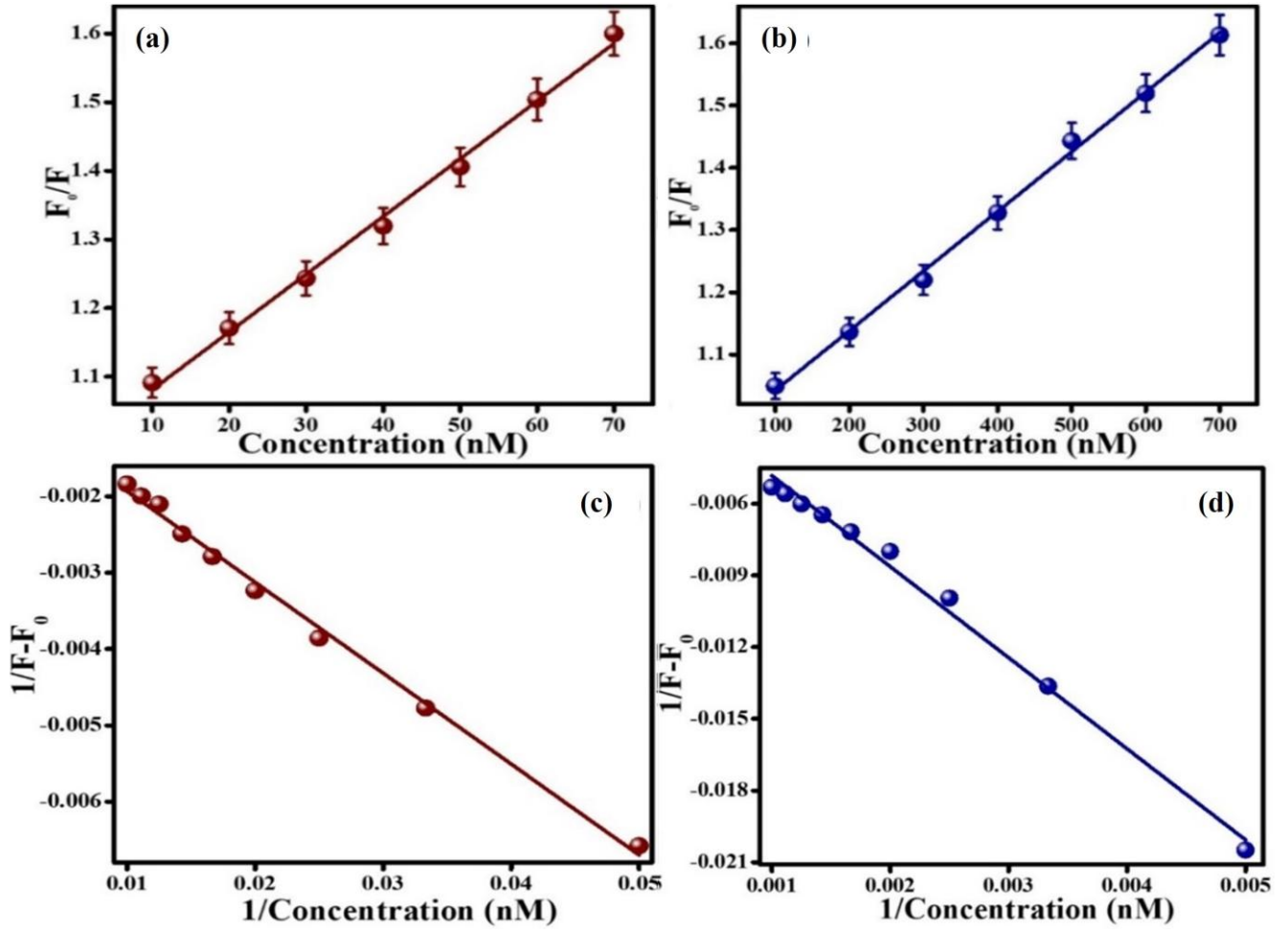


Fig. 3. (a, b) Stern-Volmer plot, and (c, d) B-H plots for FePE-Nps and FeCH-Nps, respectively.

© Ariston Publications 2025. All rights reserved.

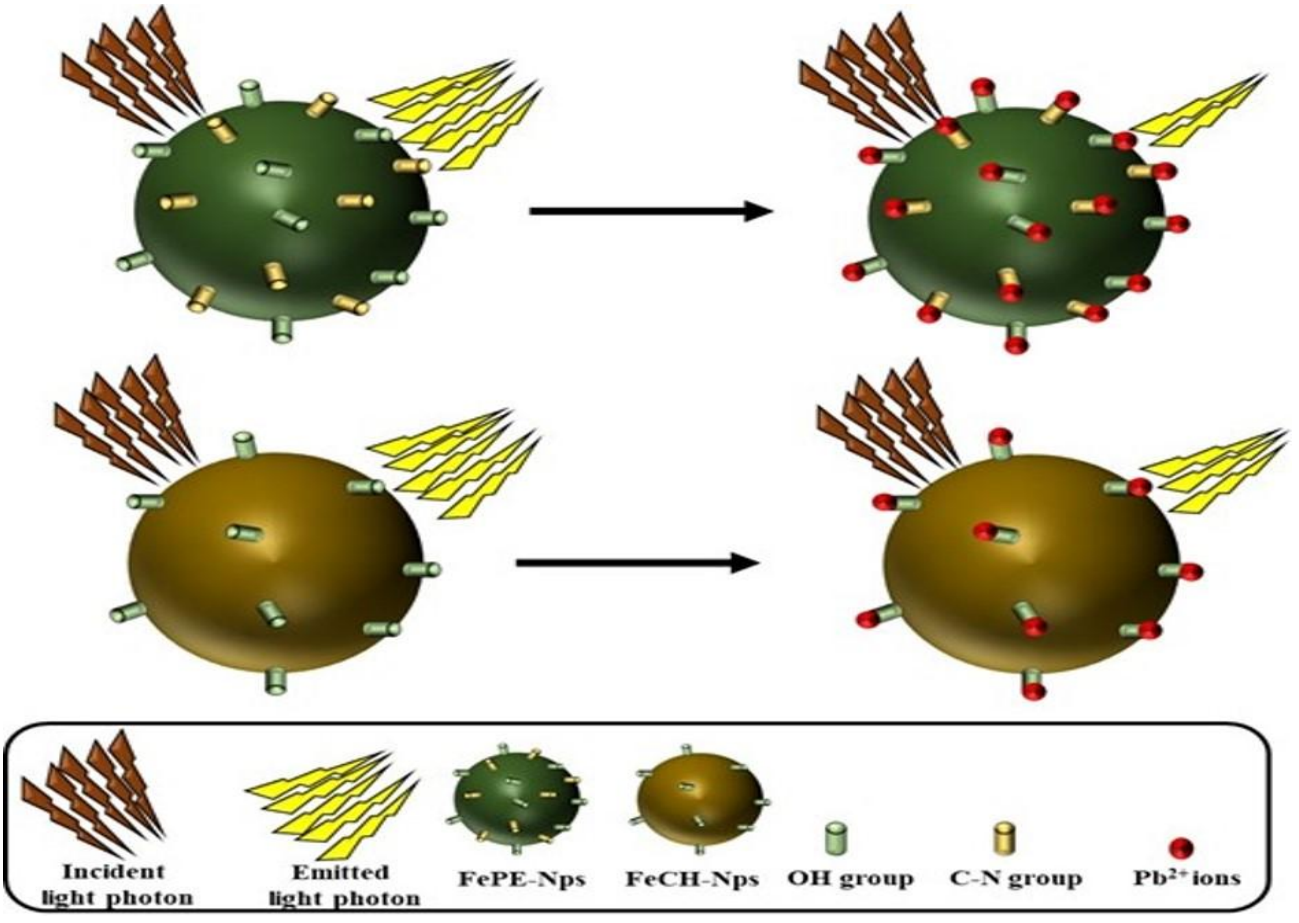


Fig. 4. Diagrammatic representation showing fluorescence quenching due to the interaction of Pb^{2+} ions with the functional groups of FePE-Nps and FeCH-Nps.

Moreover, the binding affinity of Nps towards the detected metal ions was determined by using the B-H plot which was drawn by putting the values of calculated intensity differences against the different concentrations of Pb^{2+} ions taken in increasing order (Figure 3 (c) and (d)). The values of $6.2\times10^{6}M^{-1}$ and $2.6\times10^{5}M^{-1}$ were calculated as binding constants for FePE-Nps and FeCH-Nps respectively. The larger value of binding constant obtained for FePE-Nps displayed a greater tendency of FePE-Nps to interact and form complex with Pb^{2+} ions and hence, demonstrated better sensing application than FeCH-Nps. Furthermore, the better interaction and greater efficiency of FePE-Nps enhanced its application to be used as a sensor for the detection of even the trace concentrations of Pb^{2+} ions.

3.2.2. Mechanism of sensing

The presence of Pb^{2+} ions in the solution altered the fluorescence spectrum of FePE-Nps and FeCH-Nps. The fluorescence quenching was noticed in the spectrum after the addition of Pb^{2+} ions which reflected the interactions between the concerned metal ions and Nps. As reflected in the FTIR spectrum of FePE-Nps and FeCH-Nps, hydroxyl groups were present on the surface of Nps. Pb^{2+} metal ions are reported to form different types of bonds with hydroxyl groups. So, when the concerned metal ion was added to the nanoparticles solution, it bonded with the hydroxyl group of the Nps to form a complex which resulted in the depreciated emission intensity of the Nps. The difference in the sensing efficiency of both Nps was because of the presence of the C-N group on the surface of FePE-Nps. The interaction of the nitrogen functional group of FePE-Nps with Pb^{2+} ions further reduced the luminescence intensity of the system. Since better sensing results were obtained with FePE-Nps than FeCH-Nps, therefore, our systems could serve as a better alternative for the sensing of toxic Pb^{2+} ions in water. Figure 4 shows the diagrammatic representation of the process involved in the sensing of Pb^{2+} ions.

3.2.3. Interference studies

To check the efficiency of the developed sensors in the presence of different metal ions, interference studies were conducted to mimic real environment situations. For the concerned purpose, 3 mM solutions of 14 different interfering metal salts were selected. The final solutions were prepared by sonicating the aqueous solutions of Nps containing equal concentrations of Pb^{2+} ions and other

 © Ariston Publications 2025. All rights reserved.

interfering metal ions separately. The emission spectra were recorded for the Nps solutions containing only interfering metal ions and Nps solutions containing both Pb^{2+} ions and interfering metal ions.

The comparison of the results of fluorescence emissions revealed only marginal changes in the spectrum of Nps when mixed with different metal ions. But this difference was elevated greatly in the form of quenching when the concerned solutions were mixed with Pb^{2+} ions. Hence, the excellent selectivity and sensitivity of the proposed sensors were concluded with the help of collective information gathered from Figure 5 (a). Moreover, the difference in the intensities of the bar graphs between FePE-Nps and FeCH-Nps had further authenticated the stronger association of Pb^{2+} ions with FePE-Nps, thus promoting better efficiency and applicability of greenly synthesized biocompatible sensor for the detection or sensing of pollutant from the water sources.

3.2.4. Real samples testing

The practical applicability of the proposed green and chemical sensor for Pb^{2+} ions estimation was investigated in real water samples. The realistic effectiveness of sensors was tested in the samples taken from different water sources including borewell water, tap water, rainwater, and deionized water. Based upon the detection limits calculated for FePE-Nps and FeCH-Nps, different concentrations of Pb^{2+} ions were spiked in the aqueous solutions of Nps prepared in real water samples. The sets of five concentrations were spiked in each of the samples. For FePE-Nps, Pb^{2+} ions ranging from 10-50 nM concentration were tested (Figure 5(b)) whereas for FeCH-Nps because of comparatively lower performance, relatively higher concentrations (100-500 nM) were used (Figure 5(c)). The obtained emission spectra recorded the changes in the intensities which were quantified with the help of linear calibration method. It gave an estimation of average recovery rates for the tested samples by using following formula:

$$\text{Recovery (\%)} = \frac{\text{Calculated } Pb^{2+}}{\text{Spiked } Pb^{2+}} \times 100 \quad (4)$$

The average recovery rates were found in the range of 94-98% for FePE-Nps and 90-97% for FeCH-Nps. Therefore, it was concluded that our devised systems exhibited excellent results in the real water samples, hence confirming their potential adequacy for practical applications. Moreover, the comparisons made between both the sensors advocated better results with FePE-Nps for the sensing of Pb^{2+} ions, thus sustaining the green approach for the detection of toxic pollutants.

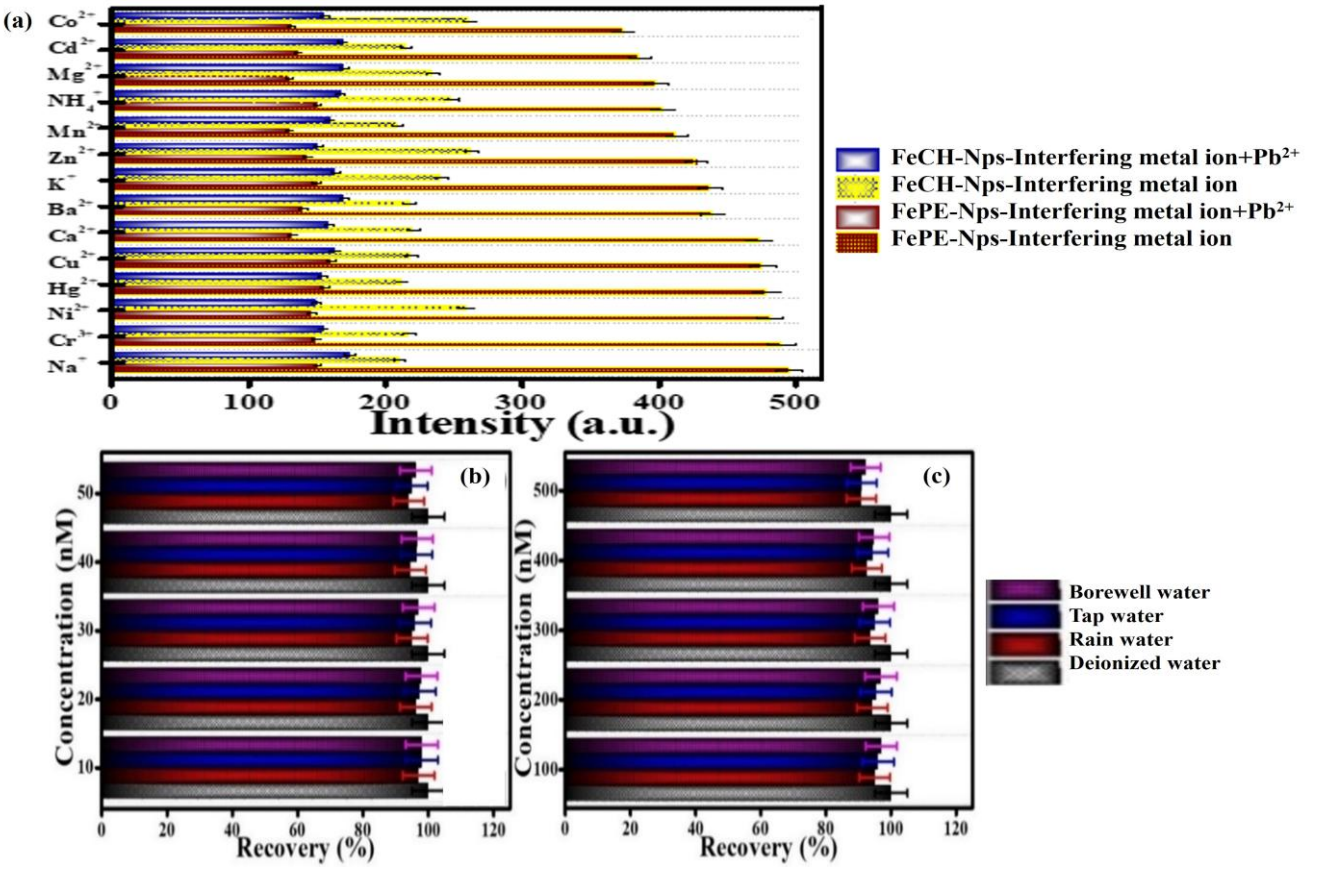


Fig. 5. (a) Emission spectra showing interference of different metal ions with Pb^{2+}, and (b, c) recovery percentages of different concentrations of Pb^{2+} ions from the real samples containing FePE-Nps and FeCH-Nps respectively.

© Ariston Publications 2025. All rights reserved.

3.2.5. Comparison with other fluorescent sensors

Various sensors have been synthesized till now by the researchers for the fluorescent detection of Pb^{2+} ions. But the limit of detection value was found to be higher in comparison of our developed sensor. For instance, Desai et al. developed as sensor based upon the combination of La^{3+} ion and bovine serum albumin gold nanoclusters for the detection of Pb^{2+} ions with the detection limit of 0.19 µM [46]. Boobalan et al. derived mushroom-based carbon dots using hydrothermal carbonization approach but the limit of detection was procured to be 58.63 µM only [47]. Sharma et al. developed functionalized molybdenum disulfide (MoS_2) quantum dots (QDs) and used as a sensitive fluorescent probe for monitoring the lead (Pb^{2+}) ions in an aqueous medium [40]. The limit of detection was calculated to be 50 µM. Anusuya et al. synthesized a sensitive sensor for the Pb^{2+} ions detection based on oxygenated functional groups decorated graphene quantum dots (GQDs) with the detection limit of 2.011 µM [48]. An et al. formulated luminescence probe based on amino-functionalized metal-organic frameworks for the selective detection of Pb^{2+} ions but the detection limit was 0.25 µM [49]. Inspite of the cost-effectiveness of our developed sensor, it also exhibits the limit of detection value of 19.57 nM which was very low as compared to the other sensors.

4. CONCLUSION

This study presents a comparative analysis of iron oxide nanoparticles synthesized via green and chemical routes for the fluorescence-based detection of lead (Pb^{2+}) ions. The results highlight that the green synthesis approach, utilizing plant extracts, offers significant advantages over conventional chemical methods. FePE-NPs exhibited enhanced sensitivity, selectivity, and stability in detecting Pb^{2+} ions, as evidenced by their lower LOD value of 19.57 nM compared to 29.43 nM for FeCH-NPs. The superior performance of FePE-NPs can be attributed to the presence of bioactive functional groups from the plant extract, which facilitate stronger interactions with Pb^{2+} ions and improve the quenching efficiency of the fluorescence sensor. Characterization studies confirmed the structural and morphological properties of both FePE-NPs and FeCH-NPs, demonstrating their stability in aqueous solutions. The fluorescence quenching mechanism was attributed to the binding interactions between Pb^{2+} ions and functional groups on the nanoparticle surface, particularly hydroxyl and nitrogen-containing moieties in FePE-NPs. Moreover, real sample testing using various water sources confirmed the high recovery efficiency of FePE-NPs (94–98%), reinforcing their potential for practical applications in environmental monitoring. A key advantage of the green synthesis approach is its sustainability, as it eliminates the need for toxic chemicals, reduces energy consumption, and produces biocompatible nanoparticles. This study underscores the viability of plant-mediated nanoparticle synthesis as a promising alternative for developing cost-effective and eco-friendly sensors for detecting toxic metal ions. Future research could explore the scalability of this method, optimization of synthesis parameters, and integration of green-synthesized nanoparticles into advanced sensor platforms for real-time environmental monitoring and industrial wastewater treatment. By leveraging the benefits of green chemistry, the development of nanoparticle-based sensors can contribute to safer water management practices and sustainable environmental remediation strategies.

DECLARATIONS

Ethical Approval

We affirm that this manuscript is an original work, has not been previously published, and is not currently under consideration for publication in any other journal or conference proceedings. All authors have reviewed and approved the manuscript, and the order of authorship has been mutually agreed upon.

Funding

Not applicable

Availability of data and material

All of the data obtained or analyzed during this study is included in the report that was submitted.

Conflicts of Interest

The authors declare that they have no financial or personal interests that could have influenced the research and findings presented in this paper. The authors alone are responsible for the content and writing of this article.

Authors' contributions

All authors contributed equally in the preparation of this manuscript.

REFERENCES

[1] Ali, M.M., Hossain, D., Al-Imran, A., Khan, M.S., Begum, M., and Osman, M.H., **2021**. Environmental pollution with heavy metals: A public health concern. *Heavy Metals - Their Environmental Impacts and Mitigation*, pp. 771-783.

[2] Al Naggar, Y., Khalil, M.S., and Ghorab, M.A., **2018**.

 © Ariston Publications 2025. All rights reserved.

Environmental pollution by heavy metals in the aquatic ecosystems of Egypt. *Open Access Journal of Toxicology*, 3(1), p. 555603.

[3] Qasem, N.A., Mohammed, R.H., and Lawal, D.U., **2021**. Removal of heavy metal ions from wastewater: A comprehensive and critical review. *NPJ Clean Water*, 4(1), pp. 1-15.

[4] Feng, X., Long, R., Wang, L., Liu, C., Bai, Z., and Liu, X., **2022**. A review on heavy metal ions adsorption from water by layered double hydroxide and its composites. *Separation and Purification Technology,* 284, p. 120099.

[5] Li, Y., Zhao, B., Duan, K., Cai, J., Niu, W., and Dong, X., **2020**. Assessments of water-soluble inorganic ions and heavy metals in atmospheric dustfall and topsoil in Lanzhou, China. *International Journal of Environmental Research and Public Health*, 17(8), p. 2970.

[6] Jaishankar, M., Tseten, T., Anbalagan, N., Mathew, B.B., and Beeregowda, K.N., **2014**. Toxicity, mechanism, and health effects of some heavy metals. *Interdisciplinary Toxicology*, 7(2), pp. 60-72.

[7] Wu, X., Cobbina, S.J., Mao, G., Xu, H., Zhang, Z., and Yang, L., **2016**. A review of toxicity and mechanisms of individual and mixtures of heavy metals in the environment. *Environmental Science and Pollution Research,* 23, pp. 8244-8259.

[8] Flora, S.J., Flora, G., and Saxena, G., **2006**. Environmental occurrence, health effects and management of lead poisoning. *Lead*, pp. 158-228.

[9] Mishra, S., Bharagava, R.N., More, N., Yadav, A., Zainith, S., Mani, S., and Chowdhary, P., **2019**. Heavy metal contamination: An alarming threat to environment and human health. *Environmental Biotechnology: For Sustainable Future*, pp. 103-125.

[10] Sall, M.L., Diaw, A.K.D., Gningue-Sall, D., Efremova Aaron, S., and Aaron, J.J., **2020**. Toxic heavy metals: Impact on the environment and human health, and treatment with conducting organic polymers: A review. *Environmental Science and Pollution Research*, 27, pp. 29927-29942.

[11] Buruiana, D.L., Lefter, D., Tiron, G.L., Balta, S., and Bordei, M., **2015**. Toxicity of heavy metals on the environment and human health. *International Multidisciplinary Scientific GeoConference: SGEM*, 5(2), pp. 565-571.

[12] Aslam, M., Aslam, A., Sheraz, M., Ali, B., Ulhassan, Z., Najeeb, U., Zhou, W., and Gill, R.A., **2021**. Lead toxicity in cereals: Mechanistic insight into toxicity, mode of action, and management. *Frontiers in plant science*, 11, p. 587785.

[13] Zulfiqar, U., Farooq, M., Hussain, S., Maqsood, M., Hussain, M., Ishfaq, M., Ahmad, M., and Anjum, M.Z., **2019**. Lead toxicity in plants: Impacts and remediation. *Journal of environmental management*, 250, p.109557.

[14] Kumar, A., Kumar, A., MMS, C.P., Chaturvedi, A.K., Shabnam, A.A., Subrahmanyam, G., Mondal, R., Gupta, D.K., Malyan, S.K., Kumar, S.S., and A. Khan, S., **2020**. Lead toxicity: health hazards, influence on food chain, and sustainable remediation approaches. *International journal of environmental research and public health*, 17(7), p. 2179.

[15] Vaziri, N.D., **2008**. Mechanisms of lead-induced hypertension and cardiovascular disease. *American Journal of Physiology-Heart and Circulatory Physiology*, 295(2), pp. H454-H465.

[16] Ferreira de Mattos, G., Costa, C., Savio, F., Alonso, M., and Nicolson, G.L., **2017**. Lead poisoning: acute exposure of the heart to lead ions promotes changes in cardiac function and Cav1. 2 ion channels. *Biophysical reviews*, 9(5), pp. 807-825.

[17] Huat, T.J., Camats-Perna, J., Newcombe, E.A., Valmas, N., Kitazawa, M., and Medeiros, R., **2019**. Metal toxicity links to Alzheimer's disease and neuroinflammation. *Journal of molecular biology*, 431(9), pp.1843-1868.

[18] Breydo, L., and Uversky, V.N., **2011**. Role of metal ions in aggregation of intrinsically disordered proteins in neurodegenerative diseases. *Metallomics*, 3(11), pp.1163-1180.

[19] Cao, Y., Deng, B., Yan, L., and Huang, H., **2017**. An environmentally-friendly, highly efficient, gas pressure-assisted sample introduction system for ICP-MS and its application to detection of cadmium and lead in human plasma. *Talanta*, 167, pp. 520-525.

[20] Kollander, B., Widemo, F., Ågren, E., Larsen, E.H., and Loeschner, K., **2017**. Detection of lead nanoparticles in game meat by single particle ICP-MS following use of lead-containing bullets. *Analytical and bioanalytical chemistry*, 409, pp. 1877-1885.

[21] Schütz, A., Bergdahl, I.A., Ekholm, A., and Skerfving, S., **1996**. Measurement by ICP-MS of lead in plasma and whole blood of lead workers and controls. *Occupational and Environmental Medicine*, 53(11), pp. 736-740.

[22] Zougagh, M., de Torres, A.G., Alonso, E.V., and Pavón, J.C., **2004**. Automatic on line preconcentration and

© Ariston Publications 2025. All rights reserved.

determination of lead in water by ICP-AES using a TS-microcolumn. *Talanta*, 62(3), pp. 503-510.

[23] Rao, K.S., Balaji, T., Rao, T.P., Babu, Y., and Naidu, G.R.K., **2002**. Determination of iron, cobalt, nickel, manganese, zinc, copper, cadmium and lead in human hair by inductively coupled plasma-atomic emission spectrometry. *Spectrochimica Acta Part B: Atomic Spectroscopy*, 57(8), pp. 1333-1338.

[24] Safari, M., Yamini, Y., Masoomi, M.Y., Morsali, A., and Mani-Varnosfaderani, A., **2017**. Magnetic metal-organic frameworks for the extraction of trace amounts of heavy metal ions prior to their determination by ICP-AES. *Microchimica Acta*, 184, pp. 1555-1564.

[25] Singh, H., Bamrah, A., Bhardwaj, S.K., Deep, A., Khatri, M., Brown, R.J., Bhardwaj, N., and Kim, K.H., **2021**. Recent advances in the application of noble metal nanoparticles in colorimetric sensors for lead ions. *Environmental Science: Nano*, 8(4), pp. 863-889.

[26] Wang, H., Yang, L., Chu, S., Liu, B., Zhang, Q., Zou, L., Yu, S., and Jiang, C., **2019**. Semiquantitative visual detection of lead ions with a smartphone via a colorimetric paper-based analytical device. *Analytical chemistry*, 91(14), pp. 9292-9299.

[27] Ding, N., Cao, Q., Zhao, H., Yang, Y., Zeng, L., He, Y., Xiang, K., and Wang, G., **2010**. Colorimetric assay for determination of lead (II) based on its incorporation into gold nanoparticles during their synthesis. *Sensors*, 10(12), pp. 11144-11155.

[28] Savitha, R., Mallelwar, P., Mohanraj, M., Renganathan, T., and Pushpavanam, S., **2022**. Adsorptive preconcentration integrated with colorimetry for ultra-sensitive detection of lead and copper. *Analytical and Bioanalytical Chemistry*, 414(14), pp. 4089-4102.

[29] Sardans, J., Montes, F., and Peñuelas, J., **2010**. Determination of As, Cd, Cu, Hg and Pb in biological samples by modern electrothermal atomic absorption spectrometry. *Spectrochimica Acta Part B: Atomic Spectroscopy*, 65(2), pp. 97-112.

[30] Tudosie, M.S., Caragea, G., Popescu, D.M., Avram, O., Serban, D., Smarandache, C.G., Tudor, C., Badiu, C.D., Socea, B., Dan Sabau, A., and Comandasu, M., **2021**. Optimization of a GF-AAS method for lead testing in blood and urine: A useful tool in acute abdominal pain management in emergency. *Experimental and Therapeutic Medicine*, 22(3), pp. 1-8.

[31] Reis, B.F.D., Knochen, M., Pignalosa, G., Cabrera, N., and Giglio, J., **2004**. A multicommuted flow system for the determination of copper, chromium, iron and lead in lubricating oils with detection by flame AAS. *Talanta*, 64(5), pp. 1220-1225.

[32] Naseri, M.T., Hosseini, M.R.M., Assadi, Y., and Kiani, A., **2008**. Rapid determination of lead in water samples by dispersive liquid–liquid microextraction coupled with electrothermal atomic absorption spectrometry. *Talanta*, 75(1), pp. 56-62.

[33] Kang, W., Pei, X., Rusinek, C.A., Bange, A., Haynes, E.N., Heineman, W.R., and Papautsky, I., **2017**. Determination of lead with a copper-based electrochemical sensor. *Analytical chemistry*, 89(6), pp. 3345-3352.

[34] Dahaghin, Z., Kilmartin, P.A., and Mousavi, H.Z., **2020**. Novel ion imprinted polymer electrochemical sensor for the selective detection of lead (II). *Food chemistry*, 303, p. 125374.

[35] Bernalte, E., Arévalo, S., Pérez-Taborda, J., Wenk, J., Estrela, P., Avila, A., and Di Lorenzo, M., **2020**. Rapid and on-site simultaneous electrochemical detection of copper, lead and mercury in the Amazon river. *Sensors and Actuators B: Chemical*, 307, p. 127620.

[36] Boonruang, S., Naksen, P., Anutrasakda, W., Chansaenpak, K., Promarak, V., Saenmuangchin, R., Phechkrajang, C., and Jarujamrus, P., **2021**. Use of nitrogen-doped amorphous carbon nanodots (N-CNDs) as a fluorometric paper-based sensor: a new approach for sensitive determination of lead (ii) at a trace level in highly ionic matrices. *Analytical Methods*, 13(32), pp. 3551-3560.

[37] Ravikumar, A., Panneerselvam, P., and Radhakrishnan, K., **2018**. Fluorometric determination of lead (II) and mercury (II) based on their interaction with a complex formed between graphene oxide and a DNAzyme. *Microchimica Acta*, 185, pp. 1-8.

[38] Saha, S.K., Ghosh, K.R., Hao, W., Wang, Z.Y., Ma, J., Chiniforooshan, Y., and Bock, W.J., **2014**. Highly sensitive and selective fluorescence turn-on detection of lead ion in water using fluorene-based compound and polymer. *Journal of Materials Chemistry A*, 2(14), pp. 5024-5033.

[39] Zhang, H., Huang, Y., Zheng, Y., Zhou, J., Wu, Q., Zhang, Z., Gan, F., and Chen, W., **2019**. Fluorescence covalent interaction enhanced sensor for lead ion based on novel graphitic carbon nitride nanocones. *Spectrochimica Acta Part A: Molecular and Biomolecular Spectroscopy*, 217, pp. 141-146.

[40] Sharma, P., and Mehata, M.S., **2020**. Rapid sensing of lead metal ions in an aqueous medium by MoS_2

 © Ariston Publications 2025. All rights reserved.

quantum dots fluorescence turn-off. *Materials Research Bulletin*, 131, p. 110978.

[41] Tian, Y., Kelarakis, A., Li, L., Zhao, F., Wang, Y., Wang, W., Yang, Q., Ye, Z., and Guo, X., **2018**. Facile fluorescence "turn on" sensing of lead ions in water via carbon nanodots immobilized in spherical polyelectrolyte brushes. *Frontiers in Chemistry*, 6, p. 470.

[42] Song, R., Zhang, Q., Chu, Y., Zhang, L., Dai, H., and Wu, W., **2019**. Fluorescent cellulose nanocrystals for the detection of lead ions in complete aqueous solution. *Cellulose*, 26, pp. 9553-9565.

[43] Huali, S.H.I., Qi, Z.H.A.O., Chao-Hui, Z.H.O.U., and Neng-Qin, J.I.A., **2022**. Nitrogen and sulfur co-doped carbon quantum dots as fluorescence sensor for detection of lead ion. *Chinese Journal of Analytical Chemistry*, 50(2), pp. 63-68.

[44] Jasrotia, T., Chaudhary, S., Kaushik, A., Kumar, R., and Chaudhary, G.R., **2020**. Green chemistry-assisted synthesis of biocompatible Ag, Cu, and Fe_2O_3 nanoparticles. *Materials Today Chemistry*, 15, p. 100214.

[45] Jasrotia, T., Dhiman, N., Sharma, N., Singh, A., Chaudhary, S., Chaudhary, G. R., and Kumar, R., **2023**. Biomonitoring and risk assessment of naturally and chemically synthesized iron-oxide nanoparticles: A comparative approach. *Science of The Total Environment*, 872, p. 161960.

[46] Desai, M.L., Basu, H., Saha, S., Singhal, R.K., and Kailasa, S.K., **2021**. Fluorescence enhancement of bovine serum albumin gold nanoclusters from La^{3+} ion: detection of four divalent metal ions (Hg^{2+}, Cu^{2+}, Pb^{2+} and Cd^{2+}). *Journal of Molecular Liquids*, 336, p. 116239.

[47] Boobalan, T., Sethupathi, M., Sengottuvelan, N., Kumar, P., Balaji, P., Gulyás, B., Padmanabhan, P., Selvan, S.T., and Arun, A., **2020**. Mushroom-derived carbon dots for toxic metal ion detection and as antibacterial and anticancer agents. *ACS Applied Nano Materials*, 3(6), pp. 5910-5919.

[48] Anusuya, T., Kumar, V., and Kumar, V., **2021**. Hydrophilic graphene quantum dots as turn-off fluorescent nanoprobes for toxic heavy metal ions detection in aqueous media. *Chemosphere*, 282, p. 131019.

[49] An, X., Tan, Q., Pan, S., Liu, H., and Hu, X., **2021**. A turn-on luminescence probe based on amino-functionalized metal-organic frameworks for the selective detections of Cu^{2+}, Pb^{2+} and pyrophosphate. *Spectrochimica Acta Part A: Molecular and Biomolecular Spectroscopy*, 247, p. 119073.

© Ariston Publications 2025. All rights reserved.